A novel Level-Set Finite Element formulation for grain growth with heterogeneous grain boundary energies.

Julien Fausty, Nathalie Bozzolo, Daniel Pino Muñoz, Marc Bernacki

MINES ParisTech, PSL Research University, CEMEF Centre de mise en forme des matriaux, CNRS UMR 7635, CS 10207 rue Claude Daunesse, 06904 Sophia Antipolis Cedex, France

Abstract

Grain coarsening in metallic material microstructures is a phenomenon usually avoided in industrial settings due to the decrease in certain physical properties of materials as the grain size increases. However, in cases where it cannot be avoided, it needs to be modeled and simulated in order to be controlled. Even so, individual grain boundaries in a material microstructure have their own structure and their own behavior and, as such, uniform grain boundary energy approaches arrive at their predictive limits when it comes to certain types of local phenomena (abnormal grain growth, thermal twinning, etc). This work presents a new heterogeneous grain boundary energy formulation for grain growth built on the thermodynamics of the phenomenon that can handle high grain boundary energy gradients. Using a full field finite element numerical framework it verifies the precision and convergence of this new formulation.

Keywords: grain growth, grain boundary energy, thermodynamics, finite element, level-set, triple junction

Email address: julien.fausty@mines-paristech.fr (Julien Fausty)

1. Introduction

Grain growth is a ubiquitous thermally activated mechanism by which the microstructures of crystalline materials coarsen at relatively high temperatures. It is a phenomenon that can be found to occur during thermal treatment operations [1, 2, 3, 4] as well as in-service at high temperatures in metallic components [5]. It is driven by the reduction of grain boundary energy [6] and, as such, is dependent upon the grain boundary character distribution as well as the grain boundary network's topology and morphology.

The thermodynamics of grain growth are relatively complex due to the so called "macroscopic" dimensionality of the grain boundaries [7]. The five dimensional space of grain boundaries is non-euclidean and partitioned into symmetric subspaces due to the inherent crystallography of the material. The topology of the grain boundary space makes it difficult to define a metric [8, 9] which makes any multivariate calculus one wishes to perform, such as that required by the finite element method (FEM), complicated.

Currently, the numerical simulation of this phenomenon is approached in multiple ways. There are probabilistic methods based on energetic descriptions of the microstructure such as Monte Carlo/Potts models [10] or some Cellular Automata based programs [11, 12, 13]. These schemes are advantageous in the relative ease of their implementation as well as the speed of their resolution. However, the pixelized description of the microstructure can be a problem if one needs to evaluate local grain boundary properties such as inclination or mean curvature. The assessment of these properties may be improved by refining the grid. However, since the grid is homogeneous, this

refinement operates on the entire simulated domain and therefore increases the computational costs consequentially. There exist deterministic methods of simulating grain growth as well which, generally, can be classified into three families: phase-field [14, 15], vertex [16] and level-set [17, 18, 19, 20] methods. The phase-field methodology is advantageous through its firm and direct foundation in the thermodynamics of the problem being solved [21]. However, in a grain growth with heterogeneous grain boundaries setting the numerical formulation becomes unstable for high grain boundary energy differences [22]. The level-set methodology is robust numerically and is easily extended to other types of interfacial problems [23, 24, 25, 26]. However, its formulation is purely kinetic and the thermodynamics are not inherent to the method.

Generally speaking, phase-field methods are more mature and more widely used in the literature for simulating grain growth than level-set schemes. Phase-field approches consist in the expression a global thermodynamic energy functional and the minimization of this functional with respect to order parameter displacements [21]. In order to consider varying properties of grain boundaries, one must make certain parameters of the phase-field simulation vary in space. These parameters must be calibrated such that the free energy integrals over the boundaries result in the correct grain boundary energies [14]. However, there is no unique way to callibrate the parameters related to the grain boundary properties in the phase-field formulation (thickness of the order parameters, depth of the energy well potentials, etc.). Also, due to the numerical instabilities of the phase-field framework, it appears difficult to introduce ratios between the lowest and highest grain boundary energies

higher than 3 or 4 [22, 27].

This work deals with the development of a level-set finite element (LS-FE) framework for grain growth with heterogeneous grain boundary energies. Even so, multiple level-set grain growth frameworks already exist. For example, in [18] the authors define a grain boundary energy "per grain" and then use an *adhoc* averaging operation to define the energy at the interface between two grains. They then solve the grain growth problem isotropically using the highest grain boundary energy followed by a mathematical procedure to correct the evolution of the grain boundary network to take into account the presence of multiple boundary energies. This approach was also studied and validated in [27]. However, this framework is almost exclusively geometric and, at the triple junctions, the authors define a seemingly arbitrary junction energy in order to obtain the correct behavior of the system. In [19] the authors solve the classic isotropic equations of grain growth using a heterogeneously valued grain boundary energy field. At the multiple junctions the isogonic point is imposed. This forces the multiple junctions to meet at equi-angles. This can be a limit in the resolution of the grain growth problem due to the fact that the angles at multiple junctions can influence the curvatures of the grain boundaries. This curvature influences the kinetics of the microstructural evolution. Even if the grain boundaries have the correct velocities considering their energies, since the curvatures are not correct, the kinetics can be inexact.

To summarize, when one considers grain growth there are many nuances of heterogeneous boundary formulations. Studies such as in [14, 19] might take into account the different energies of the grain boundaries but consider

the effect of triple junctions as negligible. Other works attempt to take into account specific properties of the multiple junctions that are either combinations of the surrounding grain boundary properties [18, 27] or intrinsic properties [22]. In any case, there are multiple different hypotheses and methods one may use to simulate grain growth with heterogeneous grain boundary energies with varying results.

The following will establish a formalized mathematical formulation of the physics of grain growth, propose a LS-FE approach to simulate the developed formulation, and attempt to validate the results using a simplified test case.

2. The physics of grain growth

Before formulating the equations related to grain growth, the constituents of a metallic material's microstructure must first be defined.

2.1. Crystallographic definitions

Considering a euclidean space Ω of arbitrary dimension D, parameterized by an orthonormal reference frame R, one may fill Ω with an idealized microstructure comprised of n grains $G_i \in \Omega$, being open spaces of Ω, such that $\mathcal{G} = \{G_i,\, i = 1, \ldots, n\}$ and a grain boundary network Γ such that:

$$\Gamma = \cup_{i=1}^{n} \partial \bar{G}_i, \tag{1}$$

where $\partial \bar{G}_i$ is the boundary of the closure of the open set G_i.

Dealing with crystalline materials, such as metals or alloys, each grain G_i is a crystallite with its own crystallographic frame $C_i = \{\boldsymbol{x}_j^i, j = 0, \ldots, D-1\}$. One often considers a reference crystallographic frame C_R (usually coincident with the general reference frame R) as well. This microstructure

assumed ideal in the sense that each grain G_i is considered devoid of defects (dislocations, point defects, etc.). Also, the scale of Ω allows for the approximation of the grain boundary network as a sharp interface as well as the consideration of continuous variables in each grain. This polycrystal formalism allows for the definition of a crystallographic orientation operator O_i of the grain G_i such that:

$$O_i : C_R \to C_i. \tag{2}$$

In this case, where the polycrystal is monophase, the orientation operator O_i is simply a rotation. As such, one may use whatever equivalent representation of a rotation in order to describe the crystallographic orientation.

The crystallography of the phase defines a symmetry group $\mathcal{S}$. As such, one may generally define crystallographic equivalence $\equiv_c$ between vectors $\boldsymbol{u}$ and $\boldsymbol{v}$ expressed in the same frames as:

$$\boldsymbol{u} \equiv_c \boldsymbol{v} \Leftrightarrow \exists S \in \mathcal{S} \,|\, \boldsymbol{v} = S(\boldsymbol{u}), \tag{3}$$

which means that each grain G_i has not one crystallographic frame C_i but $\#\mathcal{S}$, where $\#\mathcal{S}$ is the cardinality of the set $\mathcal{S}$, number of equivalent crystallographic frames and as many orientation operators.

Using these definitions, one may parameterize the description of a grain boundary. A grain boundary B_{ij} must be completely parameterized by its adjoining grains G_i and G_j. Of interest here is the morphology of the interface $\Gamma_{ij} = \bar{G}_i \cap \bar{G}_j$ as well as its crystallographic properties. As such, in the three dimensional case, one may describe each point of the grain boundary using five variables: 2 shape properties, describing the surface Γ_{ij}, as well as 3

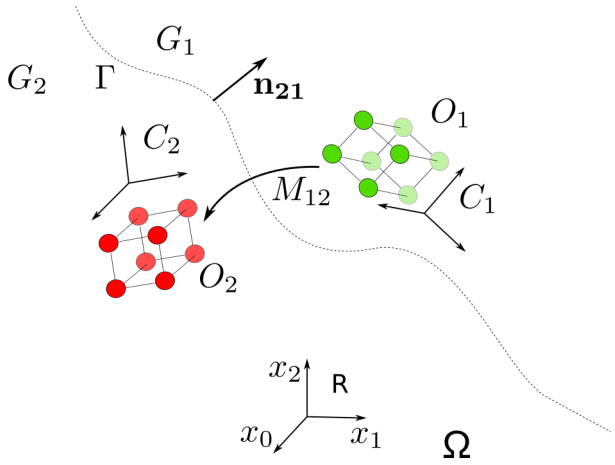

Figure 1: Schema depicting a grain boundary and its intrinsic parameters

crystallographic properties describing the passage from one crystallographic orientation O_i to another O_j. These variables are respectively the unitary normal vector from G_i to G_j:

$$\boldsymbol{n}_{ij}(X \in \Gamma_{ij}) \perp \Gamma_{ij}, \tag{4}$$

which, as a unitary vector, has only $D-1$ independent variables, that may vary along the surface Γ_{ij}, and the misorientation:

$$M_{ij} = O_i^{-1} O_j, \tag{5}$$

which represents the rotation operator that takes C_i to C_j, as illustrated in Figure 1, and has $\binom{D}{2}$ independant variables.

Therefore, in the framework defined here, any property of the grain boundary should depend on its parameters and knowing these parameters should be enough to calculate any quantity related to the grain boundary itself. However, the space of grain boundaries, being a union between a space

of unitary vectors and rotations, both stitched together by symmetries, is complex and correlations are not linear [28].

Even so, grain boundary space, being the direct product of the quotient space $\mathcal{SO}(D)/\equiv_c$ and the unit sphere $S^D \in \mathbb{R}^D$, $\mathcal{B} = \{\mathcal{SO}(D)/\equiv_c \times S^D\}$ is a smooth manifold on which one can define continuous variables [29]. In the following we will not only consider the grain boundary energy $\gamma(B \in \mathcal{B})$ continuously defined on $\mathcal{B}$ but also continuously differentiable $\gamma \in \mathcal{C}^1(\mathcal{B})$ in it.

2.2. The driving force for grain growth

In order to successfully simulate the process of grain growth, the driving forces acting on the grain boundaries must be expressed. To do so, the thermodynamics of the microstructure as a whole must be formulated and the energy of the grain boundary network must be related to the forces acting on it.

Continuing with the idealized microstructure in Ω as an isolated system, one may define the free energy F of the system at an constant temperature T, and volume V:

$$F = \int_\Omega f d\Omega, \tag{6}$$

with f the free energy density per unit volume, and $d\Omega$ an elementary volume of Ω in which the hypotheses of statistical physics are still valid.

Given that the microstructure is defined as a union of grains in $\mathcal{G}$ and a grain boundary network Γ, one may decompose its free energy F (an extensive property) into the contributions of the bulk of the grains $F_\mathcal{G}$ and the

grain boundary network F_Γ:

$$F(\Gamma, \mathcal{G}) = F_\Gamma + F_\mathcal{G}. \tag{7}$$

Furthermore, defining an energy cost per unit volume of crystal $\beta = \frac{\partial F}{\partial V}$ and an energy cost per unit surface of grain boundary $\gamma = \frac{\partial F}{\partial \Gamma}$ one may define integral expressions for the total free energy of the system:

$$F(\Gamma, \mathcal{G}) = \int_\Gamma \gamma d\Gamma + \sum_{i=0}^{n} \int_{G_i} \beta d\Omega. \tag{8}$$

As such, using an appropriate expression for the variation of the free energy of the system:

$$\delta F = \delta \left(\int_\Gamma \gamma d\Gamma + \sum_{i=0}^{n} \int_{G_i} \beta d\Omega \right), \tag{9}$$

one may distribute the variation to the individual components of the microstructure:

$$\delta F = \int_\Gamma \delta(\gamma d\Gamma) + \sum_{i=0}^{n} \int_{G_i} \delta(\beta d\Omega), \tag{10}$$

and:

$$\int_\Omega \delta(f d\Omega) = \int_\Gamma \delta(\gamma d\Gamma) + \sum_{i=0}^{n} \int_{G_i} \delta(\beta d\Omega). \tag{11}$$

Seeing as the volume of the system is constant, $V = \int_\Omega d\Omega$, one may express:

$$\int_\Omega \delta f d\Omega + f\delta(d\Omega) = \int_\Gamma \delta(\gamma d\Gamma) + \sum_{i=0}^{n} \int_{G_i} (\delta\beta d\Omega + \beta\delta(d\Omega)),$$
$$\int_\Omega \delta f d\Omega = \int_\Gamma \delta(\gamma d\Gamma) + \sum_{i=0}^{n} \int_{G_i} \delta\beta d\Omega. \tag{12}$$

The process occurring at constant temperature T and the grains being devoid of defects, the energetic cost per unit of volume of crystal β is a constant, $\delta\beta = 0$. As such:

$$\int_\Omega \delta f d\Omega = \int_\Gamma \delta(\gamma d\Gamma). \tag{13}$$

Given the principle of locality, free energy lost at one point in the microstructrue cannot be instantly found in another another point outside the first point's neighborhood. As such, using χ_Γ as the dirac function at the Γ interface:

$$\int_\Omega \delta f \chi_\Gamma d\Omega = \int_\Gamma \delta(\gamma d\Gamma). \tag{14}$$

Considering a virtual infinitesimal grain boundary displacement $\boldsymbol{\delta u}(\Gamma) = \delta u(\Gamma)\boldsymbol{n}_\Gamma$:

$$\delta f = \sum_i \left[\frac{\partial f}{\partial u_i}\delta u_i + \mathcal{O}(\delta u_i^2)\right] \simeq \frac{\partial f}{\partial \boldsymbol{u}} \cdot \boldsymbol{\delta u}, \tag{15}$$

this term can be expressed using a thermodynamic pressure jump accross the interface in the normal direction $[\![P_\Gamma]\!]$:

$$\delta f \chi_\Gamma = \frac{\partial f}{\partial \boldsymbol{u}} \cdot \boldsymbol{\delta u}\, \chi_\Gamma = [\![P_\Gamma]\!]\delta u\,, \tag{16}$$

where $[\![P_\Gamma]\!] = \frac{\partial f}{\partial \boldsymbol{u}} \cdot \boldsymbol{n_\Gamma}\, \chi_\Gamma$.

As such:

$$\int_\Omega \delta f \chi_\Gamma d\Omega = \int_\Omega [\![P_\Gamma]\!]\delta u d\Omega = \int_\Gamma [\![P_\Gamma]\!]\delta u d\Gamma. \tag{17}$$

As for the other term in equation (14):

$$\delta(\gamma d\Gamma) = \delta\gamma d\Gamma + \gamma\delta(d\Gamma), \tag{18}$$

one may express the change of area after a displacement of the surface $\delta(d\Gamma)$, where (K_ξ, K_η) represent the curvatures in the principal directions of curvature of the surface $(\boldsymbol{\tau}_\xi, \boldsymbol{\tau}_\eta)$, using the classic relationship:

$$\delta(d\Gamma) \simeq -(K_\xi + K_\eta) d\Gamma \delta u, \tag{19}$$

for which the authors present a demonstration in Appendix A.

Concerning the first term $\delta\gamma d\Gamma$ of equation (18), the calculus is more difficult. The variation of $\delta\gamma$ takes place in the grain boundary space $\mathcal{B}$ defined in the previous section. As the interface Γ changes, so too does the nature of the grain boundary $B(X \in \Gamma) \in \mathcal{B}$. In the first order:

$$\delta\gamma \simeq \frac{\partial \gamma}{\partial B} \delta B = \frac{\partial \gamma}{\partial B} \left(\frac{\partial B}{\partial M_\Gamma} \delta M_\Gamma + \frac{\partial B}{\partial \boldsymbol{n}_\boldsymbol{\Gamma}} \delta \boldsymbol{n}_\boldsymbol{\Gamma} \right). \tag{20}$$

While the variation in grain boundary energy due to the variation of the inclination of the boundary is well treated, up to the second order, in [6], there is no mention of the variation of the grain boundary energy with respect to a crystallographical transformation such as one that could occur at a triple junction as depicted in Figure 2.

Rightly so, any variation δB must be measured with respect to a metric defined in the space of grain boundaries. The definition of such a metric is a field of study within itself [9, 8] that does not have a clear answer. In the absence of the necessary mathematical tools to perform basic calculus in the misorientation space, this work proposes a simplification of the problem in which the grain boundary space $\mathcal{B}$ is short circuited and the physical space is preferred:

$$\delta\gamma \simeq \boldsymbol{\nabla}\gamma \cdot \boldsymbol{\delta u}. \tag{21}$$

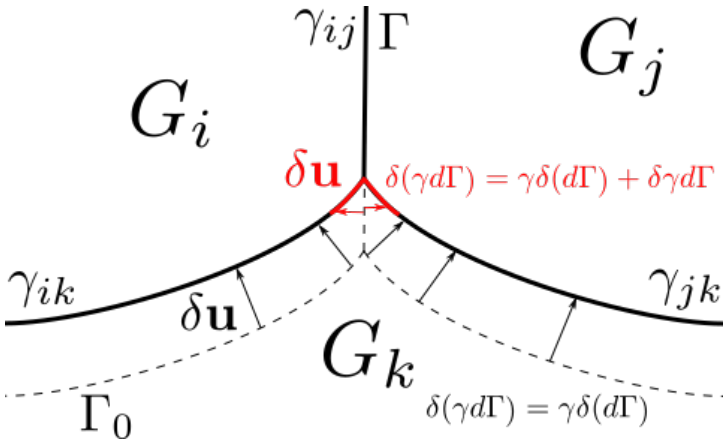

Figure 2: Schema of the movement of a triple junction leading to a change in surface length as well as a change in crystallographical nature of the boundaries.

One notable drawback of this formulation is that the system has limited knowledge of the avenues of minimization of interfacial energy open to it through all its crystallographic degrees of freedom (annealing twinning for example [30]) and therefore will not be able to exploit these avenues in its evolution. However, the system will have access to the crystallographical degrees of freedom already present locally in the microstructure. The $\boldsymbol{\nabla}\gamma$ term represents the local energetic landscape in the microstructure and allows the system to utilize those avenues, locally, in its energy minimization.

As such, combining the results of the calculations obtained in equations (14), (16), (18), (19) and (21):

$$\begin{aligned}
\delta f d\Omega &= \delta(\gamma d\Gamma),\\
[\![P_\Gamma]\!]\delta u d\Gamma &\simeq \boldsymbol{\nabla}\gamma\cdot\boldsymbol{\delta u} d\Gamma - \gamma(K_\eta + K_\xi)\delta u d\Gamma,\\
[\![P_\Gamma]\!]\delta u d\Gamma &\simeq (\boldsymbol{\nabla}\gamma\cdot\boldsymbol{n_\Gamma} - \gamma(K_\eta + K_\xi))\delta u d\Gamma,\\
[\![P_\Gamma]\!] &\simeq \boldsymbol{\nabla\gamma}\cdot\boldsymbol{n_\Gamma} - \gamma(K_\eta + K_\xi).
\end{aligned} \tag{22}$$

This thermodynamic pressure jump present along the grain boundary constitutes the driving force for grain growth. The real addition to this derivation with respect to the existing literature is the $\boldsymbol{\nabla\gamma}\cdot\boldsymbol{n_\Gamma}$ term which captures the local heterogeneity of the multiple junction. The $-\gamma(K_\eta + K_\xi)$ term corresponds to the classic driving force per unit area for growth by mean curvature.

3. The level-set FEM for grain growth

The thermodynamics expressed in the previous section result in a formulation of the driving force for grain growth with heterogeneous grain boundary energies. However, in order to simulate this phenomenon in a full field FE setting, one must evaluate this force as well as its effects on a microstructure in a discretized physical space, or mesh.

3.1. Representing the microstructure

The mathematical and numerical tools used in this work to represent the numerical microstructure have been proposed in [17] and improved in [31]. Initially, a microstructure is represented as a set of euclidean distance functions, called level-set functions, defined in the physical space Ω:

$$\Phi = \left\{ \ \phi_i(X \in \Omega) = \pm d(X,\Gamma),\ i = \{0,...,M-1\} \ \right\}, \tag{23}$$

with $d(X,\Gamma)$ the minimum euclidean distance function of a point X from a surface Γ, where $\phi_i(X) > 0$ in the grain ($X \in G_i$) and $\phi_i(X) < 0$ outside the grain ($X \notin G_i$) and M the number of level-set functions needed to represent the grains present in the microstructure. M is not necessarily equal to the number of grains in the microstructure N. For computational

efficiency reasons one may use coloring algorithms to reduce the number of level-set functions one must solve for, as in [31].

As such, one represents the grain boundary network Γ implicitly as the iso-0 values of the level-set functions. An important numerical advantage of this method is that the mesh is arbitrary, meaning that there is no need for actual nodes of the mesh to reside on the interface. However, a drawback of the method developped here, is that the level-set functions must remain true distance functions $||\boldsymbol{\nabla}\phi_i|| = 1$, in order to avoid explicit calculations of the mean curvature. This property is not necessarily conserved after a resolution increment of the convective problem:

$$\frac{\partial \phi_i}{\partial t} + \boldsymbol{v} \cdot \boldsymbol{\nabla}\phi_i = 0, \tag{24}$$

used to actually move the grain boundaries with a velocity $\boldsymbol{v}$. In order to ensure this property, a direct reinitialization algorithm is performed on all the level-set functions after each resolution increment as described in [32].

Another procedure is utilized in order to deal with possible voids, areas where all the level-set functions are negative, after a resolution increment and before reinitialization [25, 17]:

$$\phi_i(X) = \frac{1}{2}\left[\phi_i(X) - \underset{j}{max}(\phi_j(X))\right], \quad \forall i = \{0, ..., M-1\}, \forall X \in \Omega, \tag{25}$$

where voids, created at triple junctions for example, are closed by attributing the space of the void closest to each boundary to the grain behind that boundary.

An interesting property of the level-set method is the ability to define continuous fields on the entire Ω domain that describe hyper-dimensional properties, such as a grain boundary network Γ. This means that, although

this work is interested only in the evolution of the iso-0 values of the level-set functions, the variables that define this evolution are defined in the entire Ω space. This can be a challenge for certain variables defined exclusively on the grain boundary such as the misorientation M_Γ or the grain boundary energy γ_Γ.

3.2. Application to grain growth with heterogeneous grain boundary energies

In order to simulate grain growth with heterogeneous grain boundary energies in the numerical microstructure described above using the FEM, one must first define a continuous version of the driving force $[\![P_\Gamma]\!]$, defined in equation (22), acting on the grain boundaries. With the chosen sign convention and respecting the metric property $||\boldsymbol{\nabla}\phi_i|| = 1$, certain variables such as the mean curvature $\kappa = (K_\eta + K_\xi)$ or $\boldsymbol{n_\Gamma}$ (outward unitary normal) can be obtained using the following equations:

$$\boldsymbol{n_\Gamma} = -\boldsymbol{\nabla}\phi_i(X \in \Gamma), \tag{26}$$

$$\kappa = -\Delta\phi_i(X \in \Gamma), \tag{27}$$

and, as such, can easily be generalized for all $X \in \Omega$ through the level-set field. However, the grain boundary energy γ needs special treatment in order to be calculated as well as made to vary continuously in space.

3.2.1. Calculating a misorientation field

If one has a model for $\gamma(M_\Gamma, \boldsymbol{n_\Gamma})$ such as those developed in [33, 34, 35], then in order to calculate γ on the finite element mesh, one must first calculate the misorientation M_Γ and the normal to the interface $\boldsymbol{n_\Gamma}$. The normal can be found using equation (26). However, given an orientation field

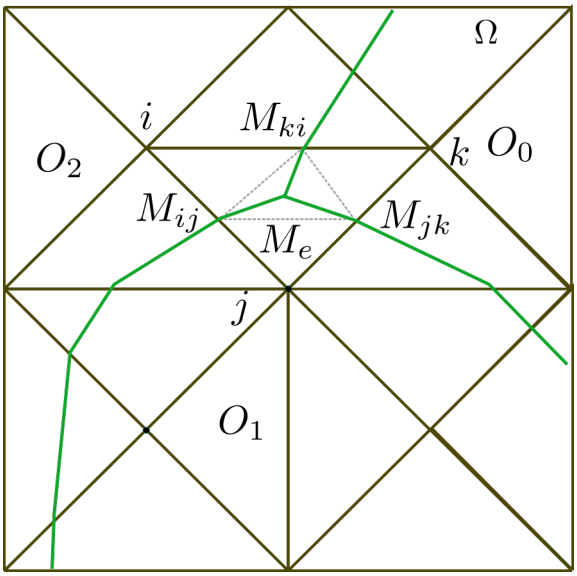

Figure 3: Schema depicting the calculation of the misorientation field at a triple junction. The dashed lines are the real zero iso-values of the three level-set functions describing the three grains.

$O(X \in \Omega)$ describing crystallographic orientations at each point in space, one must develop a procedure for computing a sufficiently representative misorientation field.

Using Figure 3 as an illustration, considering the element through which passes a grain boundary and the orientation field defined at the nodes of the mesh one can easily define the misorientation in the element as misorientation calculated between the orientation O_l on the node on one side of the boundary and O_w on the other side of the boundary such that:

$$M_{lw} = O_l^{-1} O_w, \tag{28}$$

and taking into account the minimization of the disorientation angle $\theta(O_l, O_w)$ for all possible symmetric representations of the orientations, for

$(S_i, S_j) \in \mathcal{S}^2$ the space group of the crystal:

$$M_{lw} = \underset{i,j}{\min}\, S_i^{-1} O_l^{-1} O_w S_j. \tag{29}$$

However, in an element that contains a triple junction the misorientation between three grains is undefined. A choice must be made concerning the value of the misorientation field in such an element. Very simply and arbitrarily, one can arbitrarily impose that within this element the misorientation which has the maximum disorientation angle be the misorientation in that element. This choice is potentially non-trivial regarding the results in later sections of this paper. However, the sensitivity to the values imposed at the triple junction element have been studied and been found to be negligeable. Given this choice, one can express the misorientation calculation per element as:

$$M_e = \underset{w,l}{\max}\, \underset{i,j}{\min}\, S_i^{-1} O_l^{-1} O_w S_j \quad . \tag{30}$$

One can thus ensure the correct values for misorientations in elements not traversed by grain boundaries as the identity, ensure the correct misorientation for elements traversed by one grain boundary and choose the maximal misorientation allowed in cases where the element is the seat of a multiple junction. Also, numerically, this procedure allows for a monotonic treatment of each element of the mesh which lowers the complexity of the algorithm. However, this field is extremely discontinuous in that it is valued as the identity in all elements not traversed by boundaries and given a certain value in elements that are.

3.2.2. Defining a differentiable grain boundary energy field

If one attempts to calculate $\gamma(M_\Gamma, \boldsymbol{n})$ per element of the finite element mesh, one would transport the discontinuity of the misorientation field onto the grain boundary energy field. As such, in elements traversed by grain boundaries, the γ field would have the correct value, however, in elements not traversed by grain boundaries the grain boundary energy would be zero. This, while being physically correct, introduces numerical issues in the calculation of the $\boldsymbol{\nabla}\gamma$ term defined in equation (21) which would be zero given the piece-wise constant nature of the γ field.

Seeing as the only movement that is of interest for the simulation is that of the zero iso-value of the level-set function, outside the area of Γ the values of the level-set function after a resolution increment are of little importance. As such, the only constraints on the γ field are its values at the Γ interface and its first order differentiability within the Ω domain.

With that in mind, an algorithm to construct a continuous differentiable γ_Ω field on the nodes of the finite element mesh from the γ_Γ field positively valued only at the elements traversed by Γ can be implemented. This algorithm is described in Algorithm 1.

The boundary conditions guarantee the grain boundary energy values at the grain boundaries. The resolution of a classic Laplace equation renders the field first order differentiable. The Laplace problem is solved using the FEM. Figure 4 shows an example of the fields both before and after the extension procedure at a triple junction. The triple junction remains a singularity of the field, however, the neighborhood of the junction is smoothed such that one may calculate a sufficiently approximate value of the gradient if the spatial

Algorithm 1 γ extension

$\mathcal{N}_\Gamma = \{\}$
for node n in mesh **do**
  $\gamma_{BC}(n) = 0$
  for element e connected with n **do**
    $\gamma_{BC}(n) = \max(\gamma_\Gamma(e), \gamma_{BC}(n))$
  end for
  if $\gamma_{BC}(n) \neq 0$ **then**
    put n in $\mathcal{N}_\Gamma$
  end if
end for
solve $\Delta\gamma_\Omega(X \in \Omega) = 0$ **for boundary conditions** $\gamma_\Omega(n \in \mathcal{N}_\Gamma) = \gamma_{BC}$

discretization is fine enough. Of course, with each step in the evolution of the grain boundary network, the grain boundary energy field must be recomputed with respect to the new misorientation and normal fields.

3.2.3. The weak formulation

The classical formulation for the velocities of grain boundaries in metals is [1]:

$$\boldsymbol{v} = \mu \boldsymbol{F}, \tag{31}$$

where μ is the mobility of the grain boundary, which is assumed isotropic in this work, and $\boldsymbol{F}$ the thermodynamic driving force per unit area acting on

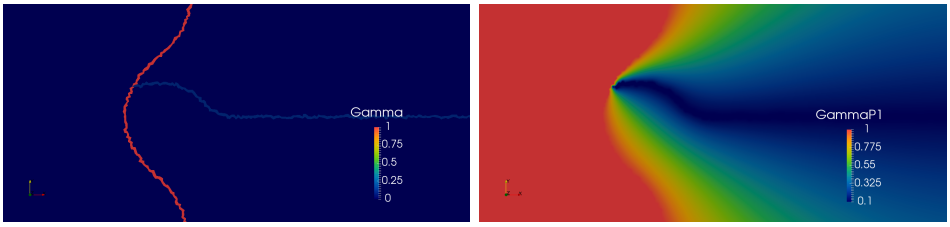

(a) (b)

Figure 4: Images showing a dimensionless γ field at a triple junction both before and after the extension procedure described in Algorithm 1.

the surface. If one inserts the expression developed in equation (22):

$$\boldsymbol{F} = [\![P_\Gamma]\!]\boldsymbol{n}, \tag{32}$$

and:

$$\boldsymbol{v} = \mu[\![P_\Gamma]\!]\boldsymbol{n} = \mu(\boldsymbol{\nabla}\gamma \cdot \boldsymbol{n} - \gamma\kappa)\boldsymbol{n}, \tag{33}$$

and then considers the transport equation (24) along with (27), (26) and $||\boldsymbol{\nabla}\phi_i|| = 1$:

$$\begin{aligned} \frac{\partial \phi_i}{\partial t} + \mu(\boldsymbol{\nabla}\gamma \cdot \boldsymbol{n} - \gamma\kappa)\boldsymbol{n} \cdot \boldsymbol{\nabla}\phi_i = 0, \\ \frac{\partial \phi_i}{\partial t} + \mu(-\boldsymbol{\nabla}\gamma \cdot \boldsymbol{n} + \gamma\kappa) = 0, \\ \frac{\partial \phi_i}{\partial t} + \mu\boldsymbol{\nabla}\gamma \cdot \boldsymbol{\nabla}\phi_i - \mu\gamma\Delta\phi_i = 0, \end{aligned} \tag{34}$$

thus constituting the strong formulation of the proposed level-set heterogeneous grain growth problem.

The weak formulation is then, with $\varphi \in H_0^1(\Omega)$:

$$
\begin{aligned}
\frac{\partial \phi_i}{\partial t}\varphi + \mu \boldsymbol{\nabla}\gamma \cdot \boldsymbol{\nabla}\phi_i \varphi - \mu\gamma\Delta\phi_i\varphi = 0,& \\
\int_\Omega (\frac{\partial \phi_i}{\partial t}\varphi + \mu \boldsymbol{\nabla}\gamma \cdot \boldsymbol{\nabla}\phi_i \varphi - \mu\gamma\Delta\phi_i\varphi) d\Omega = 0,& \\
\int_\Omega \frac{\partial \phi_i}{\partial t}\varphi d\Omega + \int_\Omega \mu \boldsymbol{\nabla}\gamma \cdot \boldsymbol{\nabla}\phi_i \varphi d\Omega - \int_\Omega \mu\gamma\Delta\phi_i\varphi d\Omega = 0,& \\
\int_\Omega \frac{\partial \phi_i}{\partial t}\varphi d\Omega + \int_\Omega \mu \boldsymbol{\nabla}\gamma \cdot \boldsymbol{\nabla}\phi_i \varphi d\Omega - \int_{\partial\Omega} \mu\gamma\varphi\boldsymbol{\nabla}\phi_i \cdot \boldsymbol{n_{\partial\Omega}} d(\partial\Omega) + \int_\Omega \boldsymbol{\nabla}(\mu\gamma\varphi)\boldsymbol{\nabla}\phi_i d\Omega = 0,& \\
\int_\Omega \frac{\partial \phi_i}{\partial t}\varphi d\Omega + \int_\Omega \mu \boldsymbol{\nabla}\gamma \cdot \boldsymbol{\nabla}\phi_i \varphi d\Omega + \int_\Omega \mu\varphi\boldsymbol{\nabla}\gamma \cdot \boldsymbol{\nabla}\phi_i d\Omega + \int_\Omega \mu\gamma\boldsymbol{\nabla}\varphi \cdot \boldsymbol{\nabla}\phi_i d\Omega& \\
- \int_{\partial\Omega} \mu\gamma\varphi\boldsymbol{\nabla}\phi_i \cdot \boldsymbol{n_{\partial\Omega}} d(\partial\Omega) = 0,& \\
\int_\Omega \frac{\partial \phi_i}{\partial t}\varphi d\Omega + 2\int_\Omega \mu \boldsymbol{\nabla}\gamma \cdot \boldsymbol{\nabla}\phi_i \varphi d\Omega + \int_\Omega \mu\gamma\boldsymbol{\nabla}\varphi \cdot \boldsymbol{\nabla}\phi_i d\Omega - \int_{\partial\Omega} \mu\gamma\varphi\boldsymbol{\nabla}\phi_i \cdot \boldsymbol{n_{\partial\Omega}} d(\partial\Omega) = 0.&
\end{aligned}
\tag{35}
$$

4. Validating the simulation methodology

This heterogeneous grain boundary energy formulation for grain growth needs to be validated in order to test its robustness as well as its precision. This grain growth model has never been used, to the authors' knowledge, and its limits must be probed in order to discuss its relevance. As such, an academic case will be simulated in order to ensure that the model gives the correct results in cases where one can theoretically calculate them.

The simulations presented in the following paragraphs were carried out using an unstructured triangular mesh with P1 type elements for the space discretization and using an implicit Euler time step resolution for the time discretization. The resolution of the convective diffusive equations were solved using a Streamline/Upwind Petrov-Galerkin stabilized method [36].

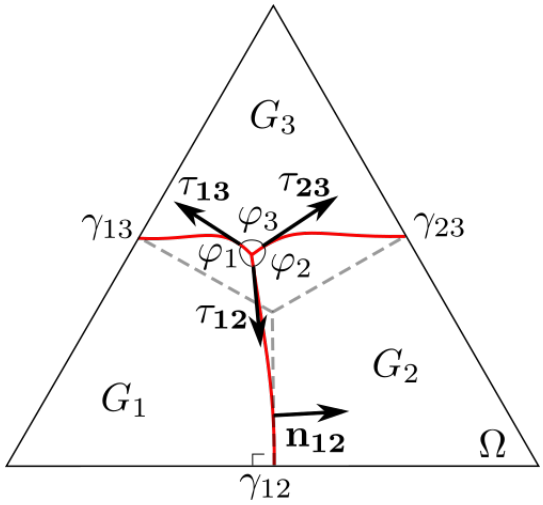

Figure 5: Illustrative diagram of the triangular test case proposed where the grain boundaries that have evolved over some time under arbitrary grain boundary energies are in red and the initial configuration of the grain boundaries is dashed.

4.1. Presentation of the test case

In order to validate the results given by the heterogeneous grain boundary energy formulation in a LS-FE framework, a dimensionless test case was constructed such that all effects **not** related to the different properties of the grain boundaries of the system were minimized. To be more precise, given a triple junction in 2D, the system must start from an initial configuration that admits a 3^{rd} order axis of rotation around the triple point. The simplest system the authors have been able to devise respecting this condition in terms of topology, length and boundary conditions is the case proposed in Figure 5.

In this case, the lengths of the three initial grain boundaries are equal at $t = 0$ and they each make 120° angles with the other two. In order for the boundary conditions to respect the 3rd order axis, the domain must have at

least three sides that form an equilateral triangle. The case is simulated with Dirichlet type boundary conditions. Therefore, the intersections of the iso-zero values of level-sets and the edges of the triangle act as fixed points. Of course, methods which rely on regular square grids will have more difficulties replicating this type of simulation. The fact this calculation was performed on a unstructured triangular cell mesh allows for more arbitrary shapes of the Ω space.

The following results will use the stationary dihedral angles obtained for a triple junction, for which one has the exact solutions depending upon the energies of the grain boundaries meeting at the junction [37] through Young's equilibrium:

$$\gamma_{12}\boldsymbol{\tau_{12}} + \gamma_{23}\boldsymbol{\tau_{23}} + \gamma_{13}\boldsymbol{\tau_{13}} = 0, \tag{36}$$

where $\boldsymbol{\tau}_{ij}$ is the tangent vector to the grain boundary Γ_{ij}. This imposes an analytical solution for the dihedral angles φ_i, $\forall i = \{1, 2, 3\}$:

$$\frac{\sin \varphi_i}{\gamma_{kj}} = C, \tag{37}$$

C being a constant for the three angles.

Also, the initial configuration is already stable with respect to an isotropic grain boundary energy case. This was also verified numerically to ensure that the formulation can also accurately simulate isotropic grain boundary energies as a special case of heterogeneous grain boundary energies.

In the following, the authors have imposed $\gamma_{23} = \gamma_{13}$ (as illustrated in Figure 5) and defined:

$$r = \frac{\gamma_{23}}{\gamma_{12}} = \frac{\gamma_{13}}{\gamma_{12}}, \tag{38}$$

as the energy ratio. By modulating r one may inject more or less heterogeneity into the system. In the literature [22] this ratio rarely supersedes 3. In order to model grain boundaries in relatively heterogeneous systems (twinned microstructures for example) the numerical formulation must be able to handle $r \approx 10$ which is the goal of this work.

4.2. Presentation of the simulations

The mesh on which this academic case is simulated is isotropic. This means that an element has approximately the same size in each direction. However, the mesh size is not the same everywhere. Mesh adaptation has been performed in a region around the triple junction in order to be able to refine the space discretization locally and not globally. This makes the simulation more computationally efficient that refining the mesh comprehensively. Figure 6 gives an idea of the mesh refinement with respect to the triple point. The time step used is imposed constant throughout a given simulation.

Multiple simulations were carried out using the case presented above while varying certain terms. However, for the sake of consistency, most parameters of the simulation do not vary. For reasons related to simplicity, the values of the parameters are dimensionless. Table 1 summarizes the parameters that do not vary in the results that follow.

4.3. Results and Analysis

The goal of this section is first, to establish whether or not the grain growth formulation for heterogeneous grain boundary energies is stable and second, to ensure that the results of the formulation are precise, in agreement

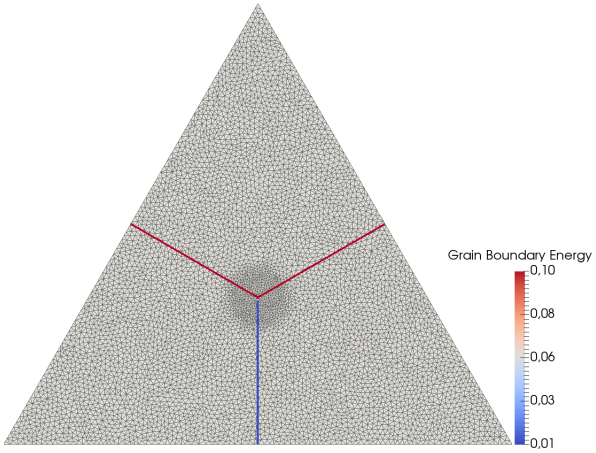

Figure 6: Initial configuration of the test case with a mesh size close to the triple junction of $h_{TJ} = 0.005$ and a mesh size outside the triple junction of $h = 0.01$ with $r = 10$.

Parameter	Value
Mobility of the grain boundaries (μ)	1
Length of the base of the domain	1
Reference grain boundary energy (γ_{23})	0.1
Radius of the refined zone (ε)	0.1
Mesh size outside the triple junction zone (h)	0.01

Table 1: Unvarying simulation parameters

with theoretical junction angles and physically consistent. As such, a sensitivity analysis to the numerical parameters of both time step Δt and mesh size h_{TJ}, the mesh size close to the triple point, is presented in order to show convergence of the method. Then, the solutions given by the simulations are studied and compared with theoretical values. The solutions using the heterogeneous grain boundary formulation for grain growth are then compared with the equivalent solutions obtained by varying grain boundary energy using the classical isotropic formulation (without a convective term), i.e.:

$$\frac{\partial \phi_i}{\partial t} - \mu\gamma(X \in \Omega)\Delta\phi_i = 0. \tag{39}$$

The classical formulation must be expressed as a weak formulation before solving it in an FE setting. However, as in the development of the heterogeneous grain growth weak formulation above, a supplemental convective term due to the variation of γ in space appears as a gradient. In the following results, "Classic" will refer to the formulation used in the majority of the current literature [18, 19, 27] using equation 39, a heterogeneous grain boundary energy field and a weak formulation tha does not integrate the heterogeneity of γ. "Weak" will refer to the classic formulation with the correct weak formulation, meaning that, as in the "Classic" case $[\![P_\Gamma]\!] = -\gamma\kappa$, however, the weak formulation is regularized to take into account the variation in the γ field. "Hetero" will be used for the fully heterogeneous formulation, being the weak formulation developped in equation (35) using equation (22).

The sensitivity analyses to both the mesh size and the time step were undertaken for two energy ratios $r = 2.5$ and $r = 0.77$ which are on either side of the isotropic case ($r = 1$). The criterion used to study the convergence and compare the simulations between each other was the error in the φ_3 angle

(in °):

$$e_{\varphi_3} = |\varphi_3^{th} - \varphi_3^{sim}| \tag{40}$$

where φ_3^{th} is the theoretical value for the φ_3 angle, given by Young's equilibrium, and φ_3^{sim} is the simulated one. The mesh sensitivity analysis was conducted using a time step of $\Delta t = 10^{-4}$ and the time step sensitivity analysis was conducted using a mesh size of $h_{TJ} = 0.001$.

The φ_3^{sim} angle was calculated automatically at each time step using the method described in Appendix B.

Both the mesh convergence and time convergence of the "Hetero" formulation can be observed in Figures 7 and 8 respectively. The simulated data is fitted using a least squares algorithm. The line equations are represented on the figures.

There is a remarkable difference in convergence between the $r < 1$ and $r > 1$ cases. Taking a closer look at the convergence exponents in both cases (the slopes of the fitted lines), the $r < 1$ case exponent is consistently about ten times smaller than the $r > 1$ for both time and space. This means that, assuming a dependence of the error on mesh size or time step $x = (h_{TJ}, \Delta t)$ of the form:

$$e_{\varphi_3} = Ax^n, \tag{41}$$

with $A(r)$ and $n(r)$, then n is around ten times smaller in the $r < 1$ case and therefore the convergence with regard to the discretization of time-space will be many orders of magnitude slower than in the $r > 1$ situation.

Figure 9b, in which the evolution of the φ_3 and $\pm e_{\varphi_3}$, where $\pm e_{\varphi_3}$ is negative if $\varphi_3^{th} < \varphi_3^{sim}$, as a function of time for many values of r is represented

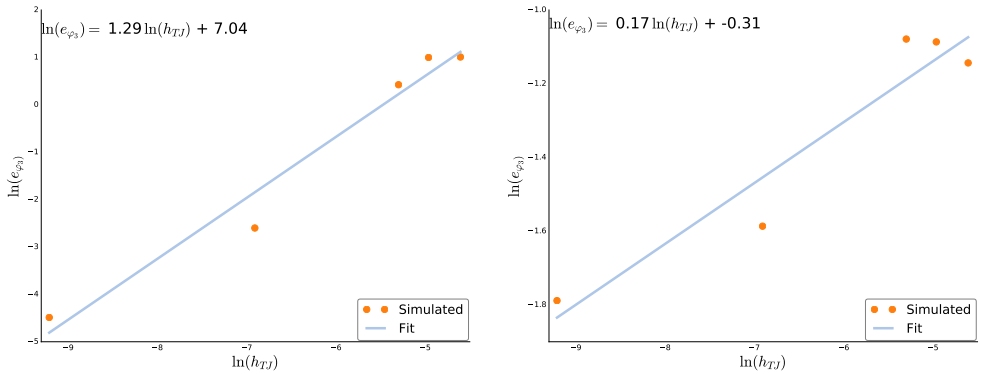

(a) $r = 2.5$ (b) $r = 0.77$

Figure 7: $\ln(e_{\varphi_3})$ as a function of mesh size $\ln(h_{TJ})$ for different energy ratios.

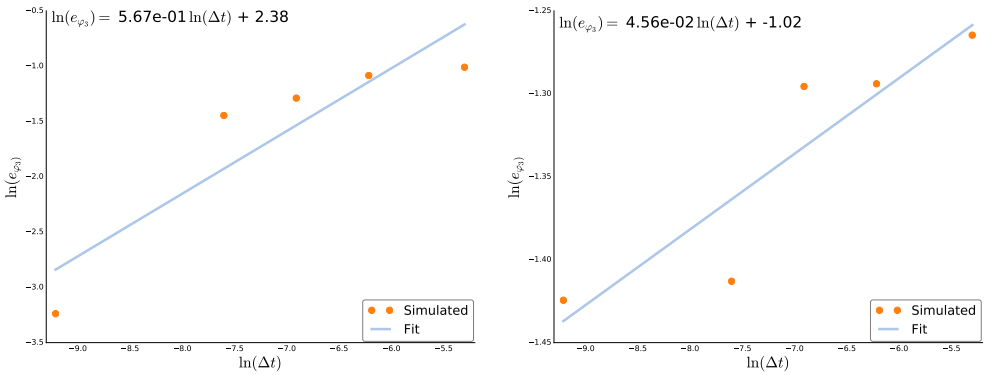

(a) $r = 2.5$ (b) $r = 0.77$

Figure 8: $\ln(e_{\varphi_3})$ as a function of mesh size $\ln(\Delta t)$ for different energy ratios.

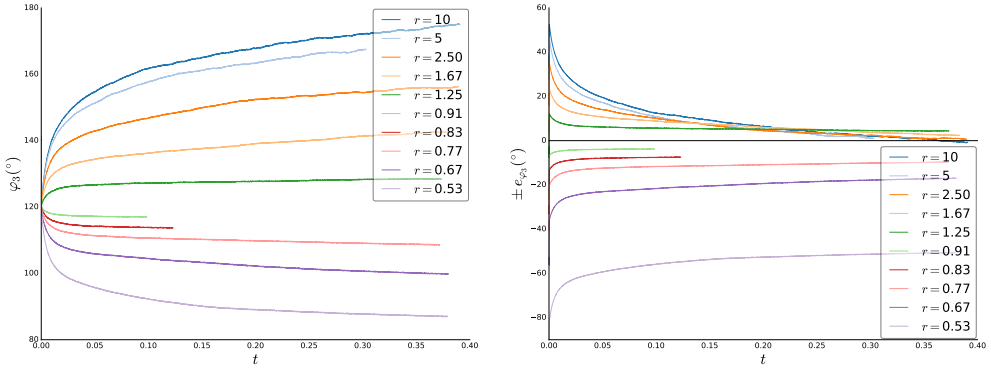

(a) φ_3 (b) $\pm e_{\varphi_3}$

Figure 9: φ_3 and $\pm e_{\varphi_3}$ as a function of t for different values of r with $h_{TJ} = 10^{-4}$ and $\Delta t = 10^{-4}$.

for the "Hetero" formulation, illustrates the results found in the convergence analysis. For r relatively close to 1, the differences between $r > 1$ and $r < 1$ are not remarkable, however, as one approaches wetting $r \approx 0.5$, the analytical value for φ_3 tends to zero, and the numerical formulation has more difficulty acheiving the desired precision. For a given tuple $(h_{TJ}, \Delta t)$ (here $(10^{-4}, 10^{-4})$), all the simulations performed in cases where $r > 1$ tend to converge towards a solution with good precision, while the simulations for which $r < 1$ arrive at a stationnary state that can be relatively far from the analytical solution. Even so, the trends in the evolutions for all simulations performed with the "Hetero" formulation diminish the error. The same cannot be said for the "Classic" or "Weak" formulations.

A graph representing the evolution of φ_3 as a function of r for all the formulations is represented in Figure 10. The best fit for the analytical dependence of φ_3 on r is clearly the new "Hetero" formulation. The "Classic"

formulation leads to φ_3 angles that are completely wrong, while the "Weak" formulation keeps the φ_3 angle around 120° regardless of the values of the grain boundary energies. Looking at the analytical solution to $\varphi_3(r)$, one can possibly explain the convergence issues for $r < 1$. Indeed, the derivative of $\varphi(r)$ becomes very steep as r tends to 0.5. It is possible that the numerical formulation of this problem has difficulties taking into account this intense gradient and either higher order terms or much smaller mesh sizes and time steps might be needed in order to get arbitrarily close to wetting.

Regarding the configuration of the triple junctions, for r much higher than 1, non-minimal energy configurations can be observed in 11a. Under the suspiscion that this was due to the Dirichlet boundary conditions, the same case was simulated with Neumann conditions (i.e. the level-set are imposed orthogonal to the border of the domain) for which the results are presented in Figure 11b. Indeed, the configuration of the triple junction seems to be more energetically appropriate with comparable values of the φ_3 angle. The reason this study was not carried out using the Neumann boundary conditions throughout is due to the dynamic nature of the simulations. Indeed, the angles arrive at a stationnary state, however, the triple junction continues to move until dissapearing outside the domain. When the triple junction approaches the borders of the domain, the automatic angle calculation developped in Appendix B stops being accurate. As such, in the Neumann boundary condition simulations, the stationnary state is more elusive.

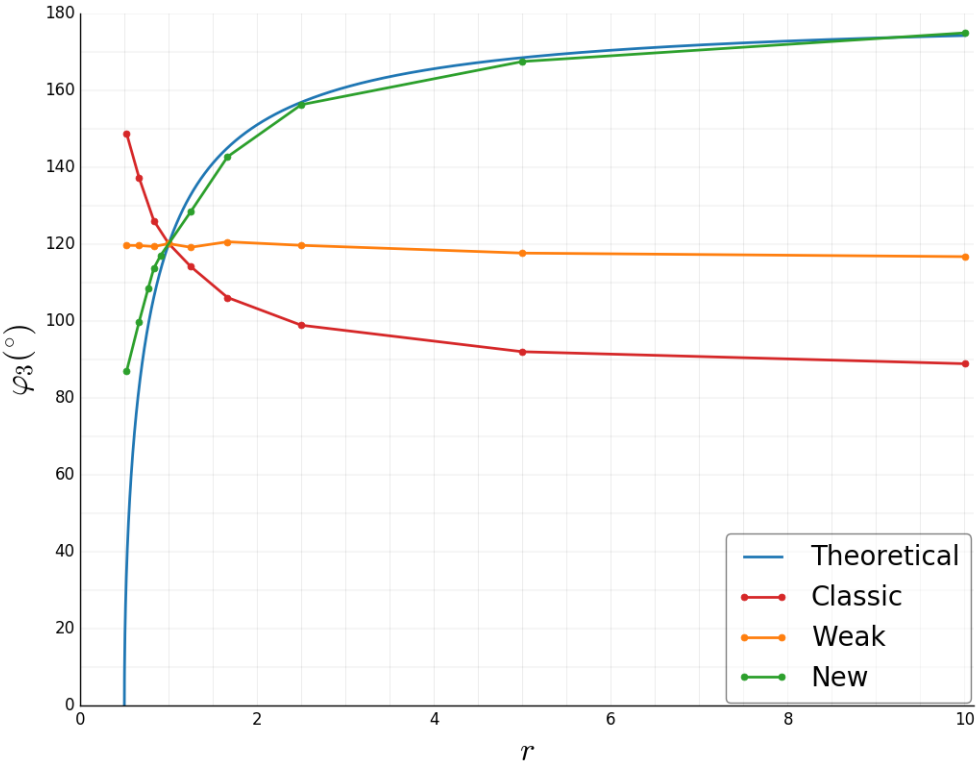

Figure 10: φ_3 as a function of r

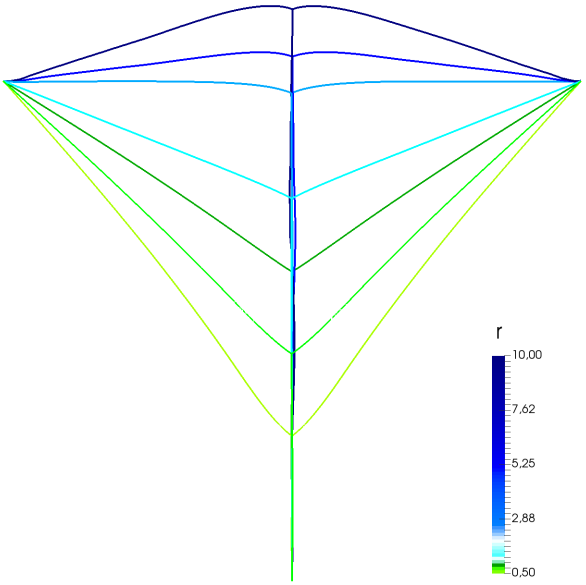

(a) Superposition of the configurations of the triple junction for different values of r

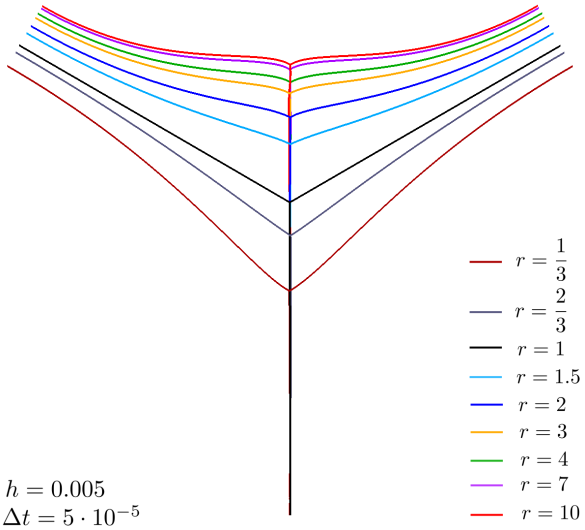

(b) Superposition of the configurations of the triple junction for different values of r using Neumann boundary conditions at $t = 0.2$.

Figure 11: Configurations of triple junctions for different boundary conditions.

5. Conclusion

A new LS heterogeneous grain boundary energy formulation for grain growth has been derived by restating the thermodynamics of the problem and taking into account a supplemental term. This formulation has been implemented in a full field FE context, with the development of crystallographical tools and methods for unstructured meshes, and tested on an academic case in order to test its precision and convergence. To the authors' knowledge, no other study has developed a numerical framework capable of simulating higher differences in grain boundary energies. The dependence of the convergence exponent on the energy ratio has been shown as well as the ability of the method to be precise at high energy ratios. In a forthcoming article the formulation will be used to model polycrystal systems with different levels of heterogneity and will be quantitatively compared with results from the literature. A large part of the discussion will be devoted to the calibration of the mesh size and time step in regards to the relevant precision that must be ensured at a triple junction in polycrystal annealing simulations.

Some perspectives of this endeavor are to extend the formulation to inclination dependent grain boundary energy models in order to capture the effects of the normal to the grain boundary. Also, texture evolutions during annealing can be studied in order to explore the effect of grain boundary properties in texture selection. Recrystallization can also be integrated into the formulation in order to start modeling twin nucleation mechanisms as well as other recrystallization phenomena. The entire formulation is theoretically valid for 3D simulations and should be generally applicable. Even so, the scale up to 3D or larger 2D simulations must be accompanied by more

intelligent time step adaptation techniques. A serious limitation to experimental validation of this work is the yet unknown exact dependance of the grain boundary energy on its five parameter description.

Acknowledgements

The authors thank Adam Morawiec, Michel Rappaz as well as Anthony Rollett for their time and valuable discussions on the topic of anisotropic grain growth. The authors also thank the group SAFRAN and the ANR (French National Research Agency) for their financial support through the OPALE industrial ANR chair.

Data Availability

The raw and processed data required to reproduce these findings cannot be shared at this time due to time limitations.

Appendix A. Virtual Surface Change

In order to express the change in surface area after a virtual displacement of the interface (see the second term of equation (18)), one can define curvilinear abscissa on the interface $\Gamma : (\eta, \xi)$, as in Figure A.12, such that:

$$d\Gamma = d\eta d\xi, \tag{A.1}$$

and:

$$\delta(d\Gamma) = d\eta\delta(d\xi) + d\xi\delta(d\eta). \tag{A.2}$$

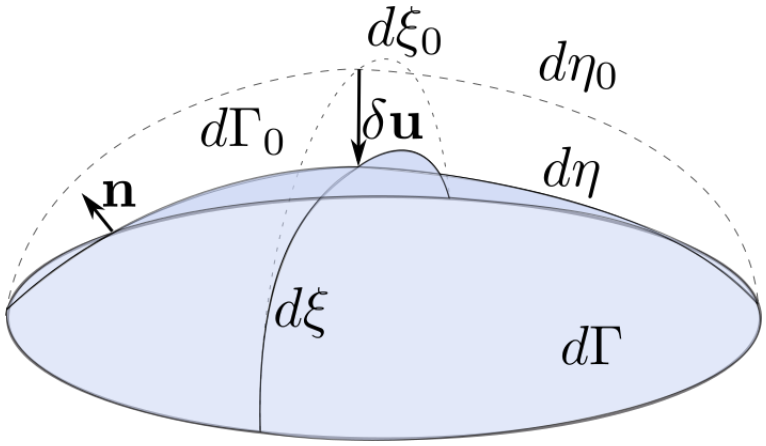

Figure A.12: Schema of the small displacement of a surface.

In a first order approximation, with the suffix 0 representing the state before displacement, one may express:

$$\begin{aligned}
\delta(d\eta) &= d\eta - d\eta_0 \\
&\simeq \sum_i \left[\frac{\partial \eta}{\partial x_i} dx_i - \frac{\partial \eta_0}{\partial x_i} dx_{i0} \right] \\
&\simeq \sum_i \left[\frac{\partial \eta}{\partial x_i} (dx_{i0} + \delta(dx_i)) - \frac{\partial \eta_0}{\partial x_i} dx_{i0} \right] \\
&\simeq \sum_i \left[\frac{\partial \eta}{\partial x_i} \delta(dx_i) + (\frac{\partial \eta}{\partial x_i} - \frac{\partial \eta_0}{\partial x_i}) dx_{i0} \right] \\
&\simeq \sum_i \left[\frac{\partial \eta}{\partial x_i} \delta(dx_i) + (\frac{\partial^2 \eta}{\partial u \partial x_i}) dx_{i0} \delta u \right] \\
&\simeq \sum_i \left[\frac{\partial \eta}{\partial x_i} \delta(dx_i) + \sum_j (\frac{\partial^2 \eta}{\partial x_j \partial x_i}) \frac{\partial x_j}{\partial u} dx_{i0} \delta u \right].
\end{aligned} \tag{A.3}$$

One may consider that the variation $\delta(dx_i)$ is negligible before the length dx_{i0} and also that any displacement of the interface can only be in the direction of the normal to the interface such that $\frac{\partial x_j}{\partial u} \delta u = n_{j0} \delta u$. Therefore:

$$\delta(d\eta) \simeq \sum_i \sum_j (\frac{\partial^2 \eta}{\partial x_j \partial x_i}) n_{j0} \delta u dx_{i0}. \tag{A.4}$$

One may express $\delta(d\xi)$ in a symmetric fashion using equation (A.2), such that:

$$\delta(d\Gamma) \simeq d\eta \sum_i \sum_j (\frac{\partial^2 \xi}{\partial x_j \partial x_i}) dx_i n_j \delta u + d\xi \sum_i \sum_j (\frac{\partial^2 \eta}{\partial x_j \partial x_i}) dx_i n_j \delta u. \quad \text{(A.5)}$$

If one considers the tangential directions $\boldsymbol{\tau_\eta}$ and $\boldsymbol{\tau_\xi}$ of the interface Γ as the directions of principal curvature, K_η and K_ξ respectively, then one may simplify the equation by expressing it in the curvilinear reference frame as:

$$\delta(d\Gamma) \simeq -K_\xi d\xi d\eta \delta u - K_\eta d\eta d\xi \delta u, \quad \text{(A.6)}$$

$$\delta(d\Gamma) \simeq -(K_\xi + K_\eta) d\Gamma \delta u. \quad \text{(A.7)}$$

Which is the classical result for the variation of surface of an interface being displaced.

Appendix B. A method for measuring angles at a multiple junction

In order to automatically measure the evolution of the angles at multiple junctions during a microstructural evolution simulation one must have two things:

1. A way to accurately track the position of a multiple junction.
2. A method for measuring the angles of a multiple junction given its position.

In a LS-FE setting, both requirements are rather simply met. In order to track the multiple junction points in a domain Ω of dimension 2, one may define a neighborhood parameter ε such the the set of points:

$$\mathcal{N}_J = \{X \in \Omega \,|\, \#\{i \,|\, \phi_i(X) < \varepsilon\} > 2\} \quad \text{(B.1)}$$

is the neighborhood of one multiple junction.

If one takes the barycenter of this neighborhood set $\mathcal{N}_\mathcal{J}$ than one obtains the multiple junction point:

$$X_J = \frac{\int_{\mathcal{N}_J} X d\Omega}{\int_{\mathcal{N}_J} d\Omega}. \tag{B.2}$$

As such, one may track the multiple junction point throughout its evolution. In order to calculate the angles created by the boundaries meeting at the junction, one may define the circle:

$$S_\varepsilon = \{X \in \Omega \,|\, d(X, X_J) = \varepsilon\}, \tag{B.3}$$

where $d(\cdot, \cdot)$ is the euclidean distance function, and the arc of the circle passing through grain G_i as:

$$S_\varepsilon^i = S_\varepsilon \cap G_i. \tag{B.4}$$

Remarking that:

$$\frac{\int_{S_\varepsilon^i} dS}{\int_{S_\varepsilon} dS} = \frac{\varepsilon\varphi_i}{2\pi\varepsilon} = \frac{\varphi_i}{2\pi}, \tag{B.5}$$

there is a simple expression for φ_i:

$$\varphi_i = 2\pi \frac{L_\varepsilon^i}{P_\varepsilon} \tag{B.6}$$

where L_ε^i is the length of the arc of S_ε^i and P is the perimeter of S_ε.

One may calculate these values on a FE mesh for a given ε and junction configuration by defining a radial distance function from the triple junction point X_J and integrating the iso-ε arcs by parts in each element. However, choosing the correct value for ε is relatively important. One would like to

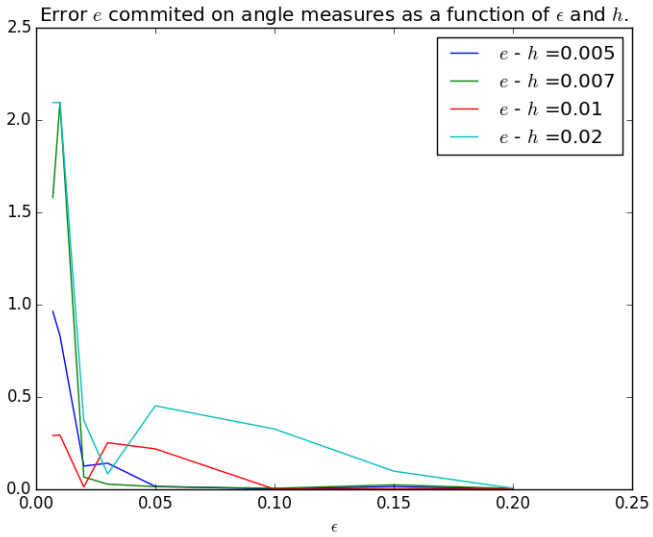

Figure B.13: Sensitivity study of the precision of angle calculations with respect to h and ε

use a ε that is as small as possible in order to be as close as possible to the junction and large enough so that the angle calculations are precise. Conducting a sensitivity analysis of the precision of the method with respect to the mesh size h, as shown in Figure B.13, one observes that $\varepsilon \approx 10h$ is sufficient for obtaining good results concerning the calculation of the angles.

One may also develop a comparable procedure for both multiple junctions in 3D using spheres as well as triple lines using cylinders.

References

[1] F. Humphreys, M. Hatherly, Recrystallization and related annealing phenomena, Elsevier, 2004.

[2] M. Akbarpour, H. Kim, Microstructure, grain growth, and hardness

during annealing of nanocrystalline cu powders synthesized via high energy mechanical milling, Materials & Design 83 (2015) 644 – 650. doi:https://doi.org/10.1016/j.matdes.2015.06.064.
URL http://www.sciencedirect.com/science/article/pii/S0264127515004141

[3] B. Milsom, H. Porwal, G. Viola, Z. Gao, M. J. Reece, Understanding and quantification of grain growth mechanism in zro2carbon nanotube composites, Materials & Design 133 (2017) 325 – 331. doi:https://doi.org/10.1016/j.matdes.2017.07.040.
URL http://www.sciencedirect.com/science/article/pii/S0264127517307086

[4] T. Omori, H. Iwaizako, R. Kainuma, Abnormal grain growth induced by cyclic heat treatment in fe-mn-al-ni superelastic alloy, Materials & Design 101 (2016) 263 – 269. doi:https://doi.org/10.1016/j.matdes.2016.04.011.
URL http://www.sciencedirect.com/science/article/pii/S0264127516304713

[5] V. Tikare, E. A. Holm, Simulation of grain growth and pore migration in a thermal gradient, Journal of American Ceramics Society 81 (1998) 480–484.

[6] C. Herring, Surface Tension as a Motivation for Sintering, Springer Berlin Heidelberg, 1999.

[7] A. Sutton, R. Ballufi, Interfaces in crystalline materials, Clarendon Press, 1995.

[8] A. Morawiec, Models of uniformity for grain boundary distributions, Journal of Applied Crystallography 42 (2009) 783–792.

[9] D. L. Olmsted, A new class of metrics for the macroscopic crystallographic space of grain boundaries., Acta Materialia 57 (2009) 2793–29799.

[10] M. Anderson, D. Srolovitz, G. Grest, P. Sahni, Computer simulation of grain growth—i. kinetics, Acta Metallurgica 32 (5) (1984) 783 – 791. doi:https://doi.org/10.1016/0001-6160(84)90151-2.

[11] Y. Liu, T. Baudin, R. Penelle, Simulation of normal grain growth by cellular automata, Scripta Materialia 34 (11) (1996) 1679 – 1683. doi:https://doi.org/10.1016/1359-6462(96)00055-3.

[12] L. Reyes, P. Pramo, A. S. Zamarripa, M. de la Garza, M. G. Mata, Grain size modeling of a ni-base superalloy using cellular automata algorithm, Materials & Design 83 (2015) 301 – 307. doi:https://doi.org/10.1016/j.matdes.2015.06.068.
URL http://www.sciencedirect.com/science/article/pii/S0264127515004189

[13] Y. Lin, Y.-X. Liu, M.-S. Chen, M.-H. Huang, X. Ma, Z.-L. Long, Study of static recrystallization behavior in hot deformed ni-based superalloy using cellular automaton model, Materials & Design 99 (2016) 107 – 114. doi:https://doi.org/10.1016/j.matdes.2016.03.050.
URL http://www.sciencedirect.com/science/article/pii/S0264127516303252

[14] K. Chang, N. Moelans, Effect of grain boundary energy anisotropy on highly textured grain structures studied by phase-field simulations, Acta Materialia 64 (2014) 443–454.

[15] I. Steinbach, Phase-field models in materials science, Modelling and Simulation in Materials Science and Engineering 17.

[16] E. A. Lazar, R. D. MacPherson, D. J. Srolovitz, A more accurate two-dimensional grain growth algorithm, Acta Materialia 58 (2010) 364–372.

[17] M. Bernacki, R. Loge, T. Coupez, Level set framework for the finite-element modelling of recrystallization and grain growth in polycrystalline materials., Scripta Materialia 64 (2011) 525–528.

[18] M. Elsey, S. Esedoglu, P. Smereka, Simulations of anisotropic grain growth: Efficient algorithms and misorientation distributions., Acta Materialia 61 (2013) 2033–2043.

[19] H. Hallberg, Y. Zhu, Stability of grain boundary texture during isothermal grain growth in $u0_2$ considering anisotropic grain boundary properties, Journal of Nuclear Materials 465 (2015) 664–673.

[20] L. Maire, B. Scholtes, C. Moussa, N. Bozzolo, D. P. Muoz, A. Settefrati, M. Bernacki, Modeling of dynamic and post-dynamic recrystallization by coupling a full field approach to phenomenological laws, Materials & Design 133 (2017) 498 – 519. doi:https://doi.org/10.1016/j.matdes.2017.08.015.
URL http://www.sciencedirect.com/science/article/pii/S026412751730761X

[21] N. Provatas, K. Elder, Phase-field methods in materials science and engineering, Wiley-VCH, 2011.

[22] E. Miyoshi, T. Takaki, Validation of a novel higher-order multi-phase-field model for grain-growth simulations using anisotropic grain-

boundary properties, Computational Materials Science 112 (2016) 44–51.

[23] H.-K. Zhao, T. Chan, B. Merriman, S. Osher, A variational level set approach to multiphase motion, Journal of Computational Physics 127 (1996) 179–195.

[24] J. Sethian, Theory, algorithms and applications of level set methods for propagating interfaces, Acta Numerica.

[25] B. Merriman, J. K. Bence, S. J. Osher, Motion of multiple junctions: A level set approach, Journal of Computational Physics 112 (1994) 334–363.

[26] Y. Wang, L. Zhang, S. Daynes, H. Zhang, S. Feih, M. Y. Wang, Design of graded lattice structure with optimized mesostructures for additive manufacturing, Materials & Design 142 (2018) 114 – 123. doi:https://doi.org/10.1016/j.matdes.2018.01.011.
URL http://www.sciencedirect.com/science/article/pii/S026412751830011X

[27] Y. Jin, N. Bozzolo, A. Rollett, M. Bernacki, 2d finite element modeling of misorientation dependent anisotropic grain growth in polycrystalline materials: Level set versus multi-phase-field method, Computational Materials Science 104 (2015) 108–123.

[28] S. Patala, C. Schuh, Topology of homophase grain boundaries in two-dimensional crystals: The role of grain exchange symmetry, Computers. Materials and Continua 17 (1) (2010) 1–17.

[29] J. M. Lee, Introduction to Smooth Manifolds, Vol. 3, Springer, 2000.

[30] B. Lin, Y. Jin, C. Hefferan, S. Li, J. Lind, R. Sutter, M. Bernacki, N. Bozzolo, A. Rollett, G. Rohrer, Observation of annealing twin nucleation at triple lines in nickel during grain growth., Acta Materialia 99 (2015) 63–68.

[31] B. Scholtes, M. Shakoor, A. Settefrati, P.-O. Bouchard, N. Bozzolo, M. Bernacki, New finite element developments for the full field modeling of microstructural evolutions using the level-set method, Computational Materials Science 109 (2015) 388–398.

[32] M. Shakoor, B. Scholtes, P.-O. Bouchard, M. Bernacki, An efficient and parallel level set reinitialization method - application to micromechanics and microstructural evolutions, Applied Mathematical Modelling 39 (2015) 7291–7302.

[33] W. T. Read, W. Shockley, Dislocation models of crystal grain boundaries, Physical Review 78 (1950) 275–289.

[34] V. V. Bulatov, B. W. Reed, M. Kumar, Grain boundary energy function for fcc metals, Acta Materialia 65 (2013) 161–175.

[35] B. Runnels, I. J. Beyerlein, S. Conti, M. Ortiz, A relaxation method for the energy and morphology of grain boundaries and interfaces, Journal of the Mechanics and Physics of Solids 94 (2016) 388–408.

[36] A. N. Brooks, A petrov-galerkin finite element formulation for convection dominated flows, Ph.D. thesis, California Institute of Technology (1981).

[37] H. Garcke, B. Nestler, B. Stoth, A multiphase field concept: Numerical simulation of moving phase boundaries and multiple junctions, SIAM Journal on Applied Mathematics 60 (1999) 295–315.